Microbial Pathogenesis 210 (2026) 108178

Contents lists available at ScienceDirect

Microbial Pathogenesis

journal homepage: www.elsevier.com/locate/micpath

Biosynthesized gold nanoparticles from *Proteus mirabilis*: A synergistic strategy against multidrug-resistant Gram-negative bacteria

Kawther Hkeem Ibrahem [a], Sazan Moffaq Abdulaziz [b], Sayran Hamad Haji [c], Aryan R. Ganjo [c,i], Nidhi Bhardwaj [d,e], Indu Bhardwaj [f], Soumya Ghosh [g,h,*]

[a] Department of Soil and Water Resources, College of Agriculture, University of Kirkuk, Kirkuk, Iraq
[b] Department of Medical Laboratory Technology, Erbil Technical Health and Medical College, Erbil Polytechnic University, Erbil, Kurdistan-Region, Iraq
[c] Department of Clinical Analysis, College of Pharmacy, Hawler Medical University, Erbil, Kurdistan Region, Iraq
[d] Center of Advanced Innovation Technologies, VŠB-Technical University of Ostrava, Ostrava, 708 00, Poruba, Czech Republic
[e] Department of Chemistry, Faculty of Science, University of Hradec Kralove, Rokitanskeho 62, 500 03, Hradec Kralove, Czech Republic
[f] Department of MLT, School of Health Science, Abhilashi University, Chailchowk, Mandi, Himachal Pradesh, 175028, India
[g] Natural and Medical Sciences Research Center, University of Nizwa, Nizwa, 616, Oman
[h] University of the Free State, Bloemfontein, 9301, South Africa
[i] Department of Medical Analysis, Faculty of Applied Science, Tishk International University, Erbil, Iraq

ARTICLE INFO

Keywords:
Antimicrobial resistance
Biosynthesis
Proteus mirabilis
Gold nanoparticles
Multi-drug resistant

ABSTRACT

Gold nanoparticles (AuNPs) are increasingly explored as antimicrobial agents for the detection and treatment of multidrug-resistant (MDR) bacterial infections. This research tries to establish an eco-friendly, biological process for synthesizing AuNPs using *Proteus mirabilis* and studies their antibacterial efficacy against MDR Gram-negative pathogens and their potential to enhance standard antibiotic efficacy. Using the Vitek-2 system, 51 *P. mirabilis* isolates were analyzed, of which 74.5 % were MDR. Netilmicin was effective against 75 % of these isolates. *P. mirabilis* extracellularly biosynthesized AuNPs, which were then characterized by XRD, FTIR, TEM, and FE-SEM. Characterization showed AuNPs measuring ~6–12 nm in size; the presence of amino and amide groups from FTIR spectra; and predominantly spherical or ellipsoidal morphology. Antibacterial activity, through broth microdilution, revealed that biosynthesized AuNPs inhibited Gram-negative bacilli at MICs of 156–1250 μg/mL. Moreover, biosynthesized AuNPs enhanced the effectiveness of antibiotics at low concentrations. Notably, when biosynthesized AuNPs were combined with ceftriaxone (commercial antibiotic), a marked synergistic effect was observed ($P < 0.0001$), with significantly enhanced prevention of pathogens compared to ceftriaxone used alone. These findings marched the function of biosynthesized AuNPs as adjuvants in drug development against MDR infections.

1. Introduction

P. mirabilis is an opportunistic bacterium associated with serious nosocomial and community-acquired infections, which are often difficult to treat due to its diverse antibiotic resistance mechanisms [1]. Among *Proteus* species, *P. mirabilis* is the most frequently isolated from clinical samples and is a major cause of complicated urinary tract infections [2]. This pathogen produces β-lactamases, particularly extended-spectrum β-lactamases (ESBLs), and can transfer genetic elements encoding these enzymes. Furthermore, mutations related to β-lactamase activity enhance its resistance to antibiotics [3]. Beyond acquired resistance to β-lactams, *P. mirabilis* exhibits intrinsic resistance to tetracyclines and polymyxins, facilitating the emergence of MDR and even extensively drug-resistant strains, which complicates clinical treatment [4]. Globally, antimicrobial resistance accounts for high annual mortality, a figure expected to rise without new intervention strategies [5]. This challenge is especially critical in developing countries, where limited surveillance and widespread misuse of antimicrobials accelerate the spread of resistance [6].

On the other hand, nanotechnology is rapidly advancing, offering immense potential in various fields, with nanomedicine emerging as a promising strategy to address antimicrobial resistance. Nanoparticles (NPs) have demonstrated strong antibacterial effects in both *in vivo* and *in vitro* studies, positioning them as potential alternatives or adjuvants to

* Corresponding author. Natural and Medical Sciences Research Center, University of Nizwa, Nizwa, 616, Oman.
E-mail addresses: soumyaghosh@yahoo.com, s.ghosh@unizwa.edu.om (S. Ghosh).

https://doi.org/10.1016/j.micpath.2025.108178
Received 23 September 2025; Received in revised form 8 November 2025; Accepted 10 November 2025
Available online 11 November 2025

conventional antibiotics. Their therapeutic potential largely stems from their unique physicochemical properties [7]. For instance, the size of NPs is comparable to bacterial cells and biomolecular systems, enabling enhanced interactions with small-molecule antibiotics [8,9]. In addition, their high surface-to-volume ratio facilitates the attachment of multiple functional ligands, leading to multivalent interactions that improve binding with target bacteria and biomolecules, making them effective self-therapeutic agents [9]. For example, Ahmeda et al. [10] prepared green-synthesized tin nanoparticles (SnNPs) using *Ziziphora clinopodioides* extract, which showed excellent anti-hemolytic anemia and hematoprotective activity in a mouse model. SnNPs enhanced blood and immune parameters, regulated inflammatory cytokines, and boosted the activities of antioxidant enzymes, all with controlled cytotoxicity. All these findings demonstrated clearly the effectiveness of SnNPs as a potential therapeutic agent for anemia and oxidative stress-related disorders. Similarly, Ahmeda et al. [11] prepared the *Lens culinaris* seed extract–conjugated AuNPs that exhibited significant anti-leukemic activity comparable to that of mitoxantrone by reducing tumor burden, altering immune responses, and showing selective cytotoxicity toward leukemic cells. These findings revealed the promising potential of these NPs as a nontoxic and effective chemotherapeutic supplement for acute myeloid leukemia. In the same way, Abassi et al. [12] also prepared a green-synthesized silver nanoparticle (Ag-NP) ointment containing *Citrus lemon* leaf extract that demonstrated excellent biocompatibility, antioxidant activity, and significantly enhanced cutaneous wound healing in pre-clinical models. Additionally, gold nanoparticles green-synthesized using *Rhus coriaria* fruit extract demonstrated potent antioxidant activity and notable cytotoxic effects against multiple esophageal cancer cell lines, with the strongest efficacy observed against human Caucasian esophageal carcinoma. Characterization confirmed uniform spherical nanoparticles (19–24 nm), supporting their stability and bioactivity.

Among the various inorganic NPs explored, such as, silver, titanium, copper, zinc, and AuNPs. AuNPs stand out due to their inert, biocompatible, and non-toxic nature [13,14]. Recent studies report that AuNPs of diverse sizes and shapes are widely applied in antibacterial therapy and anti-biofilm photothermal treatments [15]. For example, a previous study [16] synthesized AuNPs of 35, 70, and 200 nm via citrate reduction and demonstrated potent antibacterial activity of carbapenem-loaded AuNPs against carbapenem-resistant *Klebsiella pneumoniae*, *Acinetobacter baumannii*, and *P. mirabilis*. Similarly, another study [17] synthesized AuNPs from a local *P. mirabilis* isolate, characterized them by XRD, SEM, EDX, and FTIR, and reported excellent activity against MDR *Pseudomonas aeruginosa* and *Staphylococcus aureus*. Moreover, Abdoli et al. [18] prepared PVA/Gum tragacanth/graphene oxide (PVA/GT/GO) nanofiber loaded with tetracycline exhibited excellent biocompatibility, presenting high cell viability in human umbilical vein endothelial cells (HUVECs). Graphene oxide enhanced the mechanical strength, and SEM studies presented uniform fiber morphology with diameters less than 100 nm. Antibacterial tests of composite nanofiber showed that it had better antimicrobial activity compared to pure substances. In another study, Zangeneh et al. [19] prepared FeNPs@AS, which exhibited remarkable antioxidant, antibacterial, antifungal, cytotoxic, and wound-healing activities. The FeNPs@AS exhibited potent antibacterial activity against Gram-positive and Gram-negative bacteria, the most effective being against *Bacillus subtilis*, and strong antifungal activity, especially against *Candida krusei*, at $P \leq 0.01$. Characterization confirmed its stability and bioactive potential, while cytotoxicity tests indicated that it is biocompatible. These results show FeNPs@AS to be one of the few green-synthesized nanomaterials with considerable multifunctional therapeutic applications, including infection control and cutaneous wound healing.

As a result, these NPs have garnered attention in the healthcare sector [20–25] as potential substitutes or co-antimicrobial agents. Notable examples include the use of NPs to prevent catheter-associated infections, inhibit biofilm formation, employ nanoparticle therapeutics, utilize NPs in antibacterial wound dressings and coatings, as well as incorporate nano drug delivery systems [26]. Additionally, the combination of antibiotics and metal NPs in "combination therapy" has emerged as a promising solution to address the MDR crisis [27,28]. The synergistic effects of NPs and antibiotics have the potential to circumvent mechanisms of bacterial resistance to antibacterial. In contrast, nano pharmaceutical compounds with antibacterial properties not only safeguard antibiotics against molecular resistance mechanisms but also enhance the antibacterial efficacy of the antibiotic complex through the nanoparticle delivery system. This implies that conventional antibiotics can be fortified by synergistically combining them with NPs to combat MDR bacteria. In context to AuNP, a multifunctional mode of antibacterial action that increases the susceptibility of both MDR and pan-drug-resistant bacterial strains to conventional antibiotics. By forming a nano-antibiotic complex, AuNPs protect the antibiotics from the hydrolytic enzymes of the bacteria and surmount resistance mechanisms such as reduced permeability due to altered outer membrane porin proteins. The peculiar structural configuration of the nano-antibiotic complex facilitates better cellular intake and thus an effective targeting of bacterial components. Conjugation of the therapeutic agent with AuNPs could be responsible for the synergistic effect in disrupting various targets in bacteria. Notably, most traditional antibiotics and antibacterial nanomaterials induce ROS generation as a way to exert their bactericidal activity; AuNPs do not. This reduces collateral oxidative stress and makes them safer for antibacterial actions. This multi-targeting, ROS-independent mode of action underlines the potent efficacy of AuNPs against MDR bacteria [24,26,29]. Therefore, given the rising threat of MDR Gram-negative infections and limited antibiotic options, this work seeks to establish a sustainable, microbe-mediated synthesis of AuNPs and to assess their capacity to enhance antibacterial efficacy, alone and in combination with standard antibiotics.

2. Materials and methods

2.1. Collection of bacterial isolates from the clinical samples

This study involved 51 clinically confirmed isolates of *P. mirabilis* exhibiting resistance to multiple antibiotic classes, including carbapenems. The strains were collected between February 2021 and September 2022 from different clinical sources: urine (38), sputum (15), wound swabs (8), and blood (4). Additional clinical isolates of *Escherichia coli*, *Klebsiella* spp., *A. baumannii*, and *P. aeruginosa* were also obtained from Rizgari Hospital, Erbil, Kurdistan Region of Iraq, specifically for evaluating the antibacterial activity of biosynthesized AuNPs.

2.2. Clinical bacterial isolation and its molecular identification

The collected clinical samples were first processed for bacterial isolation. Cultures were grown on Trypticase Soy Agar (TSA), and pure colonies were obtained through repeated sub-culturing using the streak plate method. Isolates were identified based on morphological and biochemical characteristics, with confirmation performed using the automated Vitek-2 system (bioMérieux, USA; GN card) according to the manufacturer's instructions. Confirmed isolates were preserved as single colonies in Trypticase Soy Broth (TSB) supplemented with 20 % glycerol at −70 °C until use [30].

Bacterial genomic DNA (gDNA) extraction was performed according to the manufacturer's instructions (Promega kit, Promega Corporation Madison, WI, USA). The PCR amplification of the 16S rRNA gene was performed using primers PA-SS-F (GCGAGTCTGATGTTTGTCGC) and PA-SS-R (TAAAGGTGGCGTCGGCATTA), as described by Ref. [31]. Polymerase chain reaction (PCR) was carried out in a final reaction volume of 25 μL, comprising 3 μL of genomic DNA, 20 μL of GoTaq® Green Master Mix (Promega, USA), 1 μL of each primer (10 pmol/μL), and nuclease-free water to make up the final volume. The thermal cycling conditions included an initial denaturation at 95 °C for 2 min, followed

by 25 cycles of denaturation at 94 °C for 20 s, annealing at 58 °C for 20 s, and extension at 72 °C for 40 s. A final extension step was performed at 72 °C for 1 min [32,33].

PCR products were sequenced at the National Instrumentation Centre for Environmental Management, Seoul, Korea. The resulting nucleotide sequences were analyzed using the BLAST algorithm against available sequences in GenBank (NCBI) [34]. Isolates showing >98 % identity with previously deposited sequences were considered identified, and the confirmed sequences were subsequently deposited in GenBank to obtain accession numbers.

Furthermore, phylogenetic analysis of *P. mirabilis* isolates was conducted in MEGA 11 [35] using the Maximum Likelihood method with bootstrap support, based on 16S rRNA partial gene nucleotide sequences aligned with closely related reference sequences from GenBank.

2.3. Biosynthesis and characterization of AuNPs

The synthesis and characterization of AuNPs using *P. mirabilis* were carried out following established protocols [36,37]. A bacterial culture of *P. mirabilis* was incubated in 150 mL of sterile TSB. After incubation, the culture was centrifuged at 6000 rpm for 10 min at 4 °C, and the cell-free supernatant was collected. For AuNP synthesis, the supernatant was mixed with 10 mM chloroauric acid ($HAuCl_4$) solution (Sigma-Aldrich, USA, 99.9 %) at a 9:1 (v/v) ratio, while TSB with supernatant but without $HAuCl_4$ served as the control. Both flasks were further incubated in a shaker incubator at 37 °C and 200 rpm for 24 h. The synthesis of AuNPs by *P. mirabilis* was confirmed by visual observation, as the color of the solution changed from yellow to purple-red as determined through UV–Vis spectroscopic analysis. Following this, the prepared reaction mixture was subjected to centrifugation at 7500 rpm for a duration of 10 min in order to facilitate the separation of cellular components from the supernatant. The resultant supernatants were then carefully transferred into sterile plastic tubes. The supernatants containing the nanoparticles underwent a second centrifugation at 13,000 rpm for 5 min to facilitate the recovery of the synthesized nanoparticles. The isolated nanoparticles were subsequently resuspended in sterile distilled water and subjected to an additional centrifugation step. This procedural methodology was reiterated three times to achieve the separation of purified AuNPs. After obtaining the AuNPs, they were dried overnight at 60 °C for further characterization and applications.

Gold ion reduction was confirmed by UV–Vis spectroscopy (PerkinElmer Lambda 35). To further analyze the properties of the synthesized AuNPs, UV–visible spectra were recorded for aliquots of the culture supernatant in the wavelength range of 300–800 nm. Double-distilled water was used as a blank in this analysis. Functional groups associated with AuNP formation were analyzed by FT-IR (JASCO Spectrum 4600). The spectral range of 4000-400 cm^{-1} with a resolution of 4 cm^{-1} was analyzed. Crystalline structure and composition were determined by XRD (PAN analytical X'Pert PRO, Cu Kα radiation, $\lambda = 1.5406$ Å). The XRD measurements were performed in the 2θ range of 20°–80°, and dry powder samples of AuNPs were deposited on the XRD grid for analysis [38,39]. Particle size distribution and morphology were examined by TEM (Titan3 G2 60–300, FEI, USA, Cs corrector: image and probe) and FESEM (Quanta 4500). The sample for TEM analysis was prepared as a thin film by drop casting on a grid coated with Cu TEM holey carbon and air-dried. Chemical composition of the AuNPs was further verified using FESEM–EDX analysis. The samples were prepared and dried on a carbon-coated copper grid for this analysis.

2.4. Evaluation of antibiotic susceptibility and tolerance levels

2.4.1. Antibacterial susceptibility to conventional antibiotics

The antimicrobial panel tested included piperacillin and piperacillin–tazobactam (β-lactams); ceftazidime, ceftriaxone, and cefepime (cephalosporins); gentamicin, tobramycin, and netilmicin (aminoglycosides); ciprofloxacin and levofloxacin (quinolones); imipenem and meropenem (carbapenems); trimethoprim/sulfamethoxazole (sulfonamides); and tigecycline (tetracycline). Susceptibility of *P. mirabilis* isolates was determined using the Vitek-2 automated system according to the manufacturer's instructions [40]. Resistance phenotypes were classified as MDR following the criteria described by Ref. [41]. *E. coli* ATCC 25922 was included as the negative control.

2.4.2. Antibacterial susceptibility testing of biosynthesized AuNPs

The antibacterial activity of biosynthesized AuNPs was evaluated by determining their minimum inhibitory concentration (MIC) and minimum bactericidal concentration (MBC). Susceptibility testing was performed against clinical isolates of Gram-negative bacilli (*E. coli, Klebsiella* spp., *P. aeruginosa, A. baumannii,* and *P. mirabilis*) using the broth microdilution method, following standard protocols [42,43]. Assays were carried out in 96-well microtiter plates, where AuNPs were serially diluted in sterile Mueller–Hinton broth (MHB) from 5000 to 9.765 μg/mL. Each well was inoculated with 100 μL of bacterial suspension (0.5 McFarland $\approx 10^8$ CFU/mL), yielding a final volume of 200 μL. Plates were incubated at 37 °C for 24 h. Bacterial growth was monitored spectrophotometrically at 600 nm, with untreated bacterial cultures serving as growth controls. The MIC was defined as the lowest concentration of AuNPs that completely inhibited visible growth, while the MBC corresponded to the lowest concentration that prevented bacterial regrowth. All experiments were performed in triplicate to ensure reproducibility.

2.4.2.1. Evaluation of tolerance levels. The tolerance of clinical Gram-negative bacilli pathogens to AuNPs and standard antibiotics was evaluated following a previous method [44]. Tolerance levels were determined using the formula: Tolerance = MBC/MIC.

2.4.2.1.1. Determination of MIC of antibiotics against Gram-negative bacilli pathogens. The MICs of antibiotics against Gram-negative bacilli were determined using the broth microdilution method in 96-well microtiter plates [45]. Commercially available antibiotics such as, gentamicin (40 mg/mL), ciprofloxacin (2 mg/mL), and ceftriaxone (100 mg/mL) were used to prepare stock solutions. Each well received 100 μL of MHB, and 100 μL of antibiotic solution was added to the wells of the first row. Serial two-fold dilutions were carried out across ten wells, yielding final concentrations between 512 and 1 μg/mL. Subsequently, 10 μL of a bacterial suspension adjusted to a 0.5 McFarland standard was inoculated into each well. Two columns served as positive and negative controls. Plates were incubated at 37 °C for 18–24 h, and turbidity was assessed visually against a dark background. The MIC was defined as the lowest antibiotic concentration showing no visible growth relative to controls. All experiments were conducted in duplicate, and mean values were recorded.

2.4.2.1.2. Determination of MBC of antibiotics against Gram-negative bacilli pathogens. The MBC of antibiotics against Gram-negative bacilli was determined according to a previous study [46].

2.4.3. Combined assessment of antibiotics and AuNPs against Gram-negative bacilli

The antimicrobial activity of AuNPs (5000 μg/mL) was assessed using the standardized broth microdilution method, as described previously [47]. For the combination assay, bacterial cells were grown in MHB, and 20 μL of AuNPs (5000 μg/mL) was added to each well of a 96-well plate containing 160 μL of MHB and 20 μL of antibiotic solution. Cultures were incubated at 35 °C for 20 h. Bacterial growth was measured by optical density (OD) at 600 nm and compared against controls with antibiotics alone, AuNPs alone, or no treatment. The antibiotics tested were gentamicin (40 mg/mL), ciprofloxacin (2 mg/mL), and ceftriaxone (100 mg/mL), evaluated in combination with AuNPs at concentrations of 512 + 2500, 256 + 1250, 128 + 625, 64 + 312.5, 32 + 156.25, 16 + 78.125, 8 + 39.06, and 4 + 19.53 μg/mL, as previously reported [45].

2.5. Statistical analysis

Data were analyzed using GraphPad Prism, and statistical significance was determined by the chi-square test at $p < 0.05$.

3. Results and discussion

3.1. Epidemiological and clinical characteristics of P. mirabilis isolates

The study examined demographic variables and bacterial isolate characteristics, confirming 51 MDR isolates of *P. mirabilis* from various clinical samples. Statistical analysis indicated no significant correlation between gender, age groups, and clinical sample type ($p > 0.05$) (Table 1). Epidemiological assessment based on sex, age, and specimen type showed that 52.9 % of isolates were from female patients and 47.0 % from male patients. Age-wise, the highest proportion of isolates (41.1 %) occurred in patients aged 40–60 years, while the lowest (9.8 %) was in the 10–20-year group. Specimen analysis revealed urine as the predominant source (64.7 %), followed by swabs (23.5 %) and sputum (11.7 %). Previous studies have indicated that urinary tract infections (UTIs), such as cystitis and pyelonephritis, are commonly associated with asymptomatic bacteriuria, particularly among elderly individuals and patients with type 2 diabetes. These infections, if left untreated or inadequately managed, may lead to bacteremia and, in severe cases, progress to urosepsis, a potentially life-threatening condition. Moreover, *P. mirabilis* has been specifically implicated in the development of urinary stones (urolithiasis), further complicating the clinical course of UTIs [48,49]. In the present study, the majority of clinical isolates were recovered from urine samples, suggesting a predominance of UTIs. These findings are consistent with previous research [50] conducted in Iraq, that reported a high prevalence of *Proteus* spp. in urine samples collected from 30 clinical cases in hospitals across Baghdad. That study also found a slightly higher incidence among female patients (56 %) compared to males (43 %), with infections observed across a range of age groups. Similarly, a more recent study conducted in 2022 in Thi-Qar province, Iraq, reported a female infection rate of 52.4 % and a male infection rate of 47.6 %, with individuals aged 44 years and older being the most frequently affected by *P. mirabilis*. Furthermore, the same study identified urinary tract infections as the primary source of *P. mirabilis* isolates, accounting for 45 % of cases [51]. However, contrasting results were observed in a Taiwanese study by Lin et al. (2019), which found that among 101 *P. mirabilis* clinical isolates, the highest numbers were obtained from sputum (9 isolates), followed by urine (8 isolates), and swab samples (6 isolates). The predominance of UTI-related isolates in our findings may be attributed to the organism's strong ability to colonize the surface of urinary catheters, as well as its natural presence in the human gastrointestinal tract, which increases the likelihood of ascending urinary infections. This aligns with the classification of *P. mirabilis* as the third most common cause following *E. coli* and *K. pneumoniae*, of complicated UTIs, contributing to approximately 12 % of such infections [52].

Overall, the results indicate that clinical specimen type is the primary determinant of *P. mirabilis* isolation frequency, followed by patient sex and age group.

Table 1
Clinical and demographic characteristics of *P. mirabilis* isolates (n = 51).

Variables	No.	%
Sex		
Male	24	47
Female	27	52.9
Age		
10–20	5	9.8
20–40	14	27.4
40–60	21	41.1
60–80	11	21.5
Clinical specimen		
Urine	33	64.7
Swab	12	23.5
Sputum	6	11.7

p-value 0.058.

3.2. Sequencing analysis of the 16S rRNA gene of AuNP-producing P. mirabilis

BLAST analysis of the 16S rRNA gene sequences from the Erbil-Iraq isolates demonstrated a 98.60 % similarity to *P. mirabilis* reference strains from various global sources. Conserved 16S rRNA motifs characteristic of the *Proteus* genus were also identified across all four isolates. Pairwise sequence alignments revealed minor nucleotide differences, which may indicate regional genetic variations [43]. The sequence quality and coverage were adequate to support accurate molecular identification, consistent with criteria described in previous studies [33]. Phylogenetic analysis further confirmed the classification of these isolates as *P. mirabilis* (Fig. 1). The sequences were deposited in GenBank under accession numbers OQ975835, OQ975836, OQ975837, and OQ975838, with isolate OQ975835 identified as a novel AuNP-producing *P. mirabilis* strain.

3.3. Preparation and characterization (UV–Visible, XRD, FTIR, FE-SEM, EDX, and TEM analyses) of P. mirabilis gold nanoparticles

The cell-free supernatant of *P. mirabilis* cultures was incubated with chloroauric acid ($HAuCl_4$) solution, resulting in the reduction of Au^{3+} ions to AuNPs within 24 h at 37 °C. A visible color change from pale yellow to dark red confirmed the extracellular synthesis of AuNPs (Fig. 2A).

UV–Visible spectroscopy was performed in the 300–800 nm range to characterize the nanoparticles. A sharp absorption peak at 540 nm was observed after 24 h, indicative of surface plasmon resonance (SPR) associated with AuNP formation. This finding supports earlier reports that AuNPs typically exhibit SPR in the 520–560 nm range [53–55]. The observed color shift from yellow to pinkish-purple further confirmed gold ion reduction and nanoparticle synthesis, likely mediated by NADH-dependent nitrate reductase [28].

X-ray diffraction (XRD) analysis revealed four characteristic diffraction peaks at 2θ values of 38.00°, 44.22°, 64.55°, and 77.28°, corresponding to the (111), (200), (220), and (311) planes of a face-centered cubic (fcc) lattice of gold (JCPDS 98-005-3763) (Fig. 2B). The strong (111) reflection indicated preferential orientation and high crystallinity of the AuNPs. Using the Scherrer equation [56,57], the average crystallite size was estimated at 12.5 nm, which is in agreement with previous studies synthesizing AuNPs via *P. mirabilis* and *Arthrobacter* strains [58,59].

Fourier-transform infrared (FTIR) spectroscopy (400–4000 cm^{-1}) confirmed the presence of functional biomolecules associated with nanoparticle stabilization (Fig. 2C). Prominent peaks at 3260.07 cm^{-1} (–NH stretching, proteins), 1636.3 cm^{-1} (amide I), and 1043.3 cm^{-1} (S=O stretching, sulfoxides) indicated that proteins and other biomolecules acted as capping agents. These results were consistent with earlier findings that proteins contribute to AuNP stabilization by binding through amide groups and secondary structural modifications [17,58,60,61].

Field-emission scanning electron microscopy (FE-SEM) showed that the AuNPs were predominantly spherical to ellipsoidal with smooth surfaces and uniform distribution (Fig. 2D). Energy-dispersive X-ray spectroscopy (EDX) analysis confirmed the presence of gold, with strong signals at ~2 eV and 9 eV, alongside copper peaks attributed to the supporting TEM grid [62,63].

Transmission electron microscopy (TEM) further characterized the AuNPs at a 50 nm scale (Fig. 2E). The nanoparticles exhibited spherical, rod-like, and irregular morphologies, with slight agglomeration due to electrostatic interactions. ImageJ and Origin 9 analysis estimated an

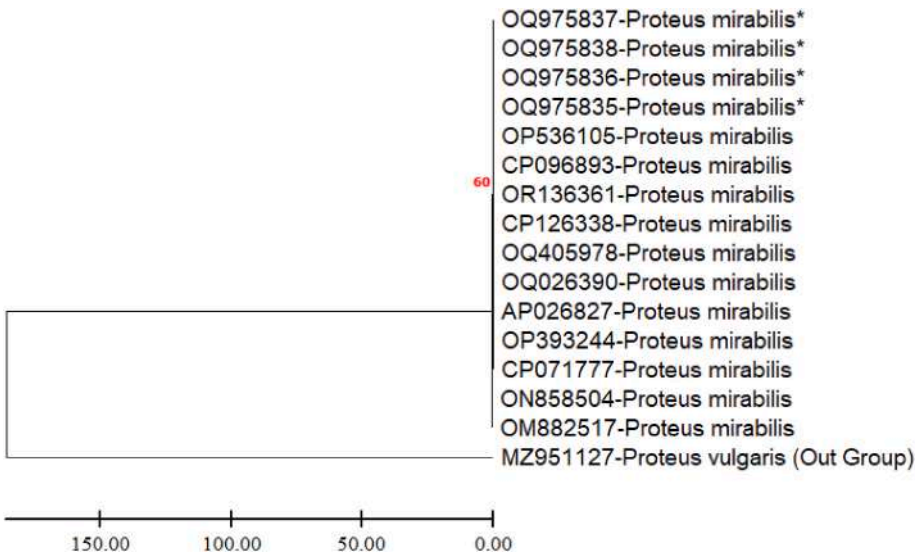

Fig. 1. Phylogenetic positioning of the four *Proteus mirabilis* isolates was determined using the Maximum Likelihood method with bootstrap analysis in MEGA 11, based on 16S rRNA partial gene sequences compared with similar sequences available in GenBank.

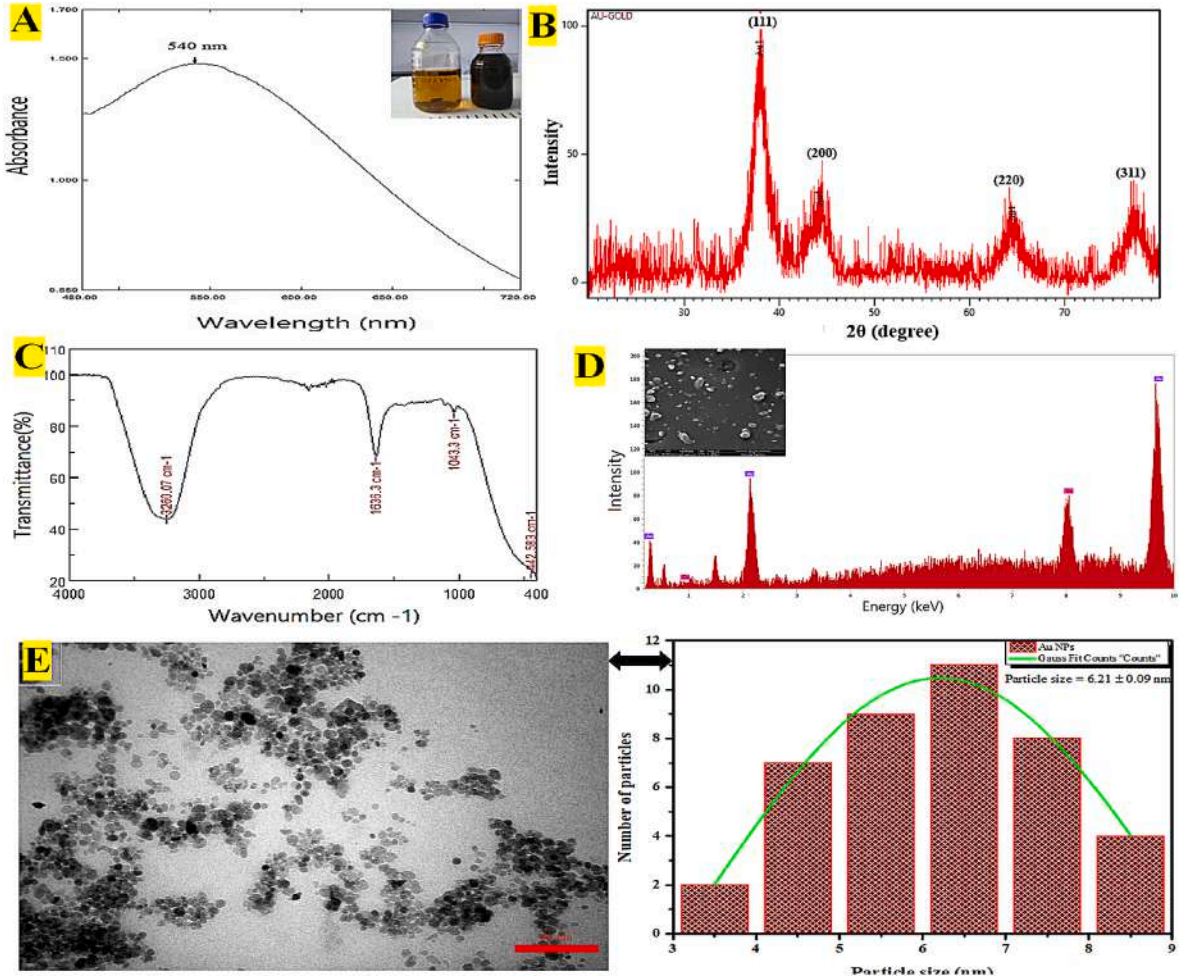

Fig. 2. Characterization of synthesized Au NPs. (A) UV–Vis absorption spectrum showing a surface plasmon resonance peak at 540 nm, inset shows the color change of the solution. (B) X-ray diffraction (XRD) pattern indicating crystalline nature with (111), (200), (220), and (311) planes. (C) FTIR spectrum showing functional groups involved in NPs stabilization. (D) Energy-dispersive X-ray (EDX) spectrum confirming elemental composition, inset displayed SEM image of Au NPs. (E) TEM image displayed particle morphology and size distribution, with average particle size of 6.21 ± 0.09 nm.

average particle size of 6.21 nm. High-resolution TEM revealed clear lattice fringes, consistent with previously reported nanostructures synthesized by bacterial and plant systems [64–66].

3.4. Resistance patterns and tolerance characteristics

3.4.1. Resistance profiles to conventional antibiotics

Analysis using the Vitek-2 automated system revealed that all 51 clinical isolates of *P. mirabilis* exhibited high resistance levels. The resistance and susceptibility profiles of these isolates are summarized in Table 2. Notably, significant variation was observed in their resistance patterns across the different antimicrobial agents tested ($p < 0.0001$).

The resistance rates of *P. mirabilis* isolates to different antibiotic classes were as follows: tigecycline (88.2 %) > imipenem (70.5 %) > ceftriaxone (58.8 %) > piperacillin (56.9 %) > gentamicin (54.9 %) > cefepime (52.9 %) > ceftazidime (50.9 %) > piperacillin/tazobactam (49 %) > ciprofloxacin (35.8 %) > trimethoprim/sulfamethoxazole and meropenem (27.4 %) > tobramycin (23.5 %) > levofloxacin (21.5 %) > netilmicin (15.6 %). Overall, 74.5 % of the isolates were classified as MDR (Table 2).

The present analysis demonstrated that the highest level of resistance was recorded against tigecycline, with 88.2 % (45/51) of isolates exhibiting resistance within the tetracycline class of antibiotics (Table 2). This observation is consistent with earlier reports [2,51] that similarly revealed that all *P. mirabilis* isolates tested displayed resistance to tigecycline. Such findings reinforce growing concerns regarding the persistence and spread of antimicrobial resistance in this species. Recent studies have highlighted the role of plasmid-mediated gene transfer in facilitating the dissemination of resistance determinants among *P. mirabilis* populations. Coupled with its well-documented intrinsic resistance to colistin, nitrofurans, tigecycline, and tetracycline, as well as its increasing resistance to extended-spectrum β-lactamases (ESBLs), *P. mirabilis* is increasingly being recognized as a clinically significant pathogen and an emerging threat to healthcare systems [67].

Notably high resistance to tigecycline may be linked to the AcrAB efflux pump (resistance-nodulation-division family), which confers resistance to multiple antibiotics, dyes, detergents, and lipophilic agents [68,69]. For instance, in May 2019, researchers in Jiangsu, China, isolated a tigecycline-resistant *P. mirabilis* strain (RGF134-1) from swine fecal samples carrying a tmexCD1-toprJ1-like gene. Confirmation by PCR, MALDI-TOF MS, and WGS revealed multidrug resistance, including resistance to tetracycline, kanamycin, amoxicillin, streptomycin, enrofloxacin, oxytetracycline, doxycycline, and tigecycline [70]. Similarly, a previous study [71] reported a 10.57 % prevalence of *P. mirabilis* among 500 clinical samples in Bangladesh, with resistance rates of 27.03 % for tigecycline, 24.32 % for fosfomycin, 21.62 % for imipenem, and 78.38 % for amikacin. Alarmingly, 75.68 % of the isolates were MDR, 13.51 % XDR, and 10.81 % PDR. Resistance determinants identified included fosA (77.78 %), fosA3 (44.44 %), fosA4 (22.22 %), NDM-1 and OXA-10 (62.5 %), NDM-2, OXA-23, and OXA-48 (50 %), and OXA-58 (25 %).

Table 2
Antimicrobial resistance profiles of *P. mirabilis* clinical isolates determined using the Vitek-2 automated system.

Antibiotics classes	Antibiotics	Resistance rates
Carbapenem	Imipenem	36 (70.5 %)
	Meropenem	14 (27.4 %)
Cephalosporin	Ceftazidime	26 (50.9 %)
	Cefepime	27 (52.9 %)
	Ceftriaxone	30 (58.8 %)
Penicillin	Piperacillin	29 (56.9 %)
	Piperacillin/tazobactam	25 (49 %)
Sulfonamides	Trimethoprim/Sulfamethoxazole	14 (27.4 %)
Tetracycline	Tigecycline	45 (88.2 %)
Quinolones	Levofloxacin	11 (21.5 %)
	Ciprofloxacin	13 (25.4 %)
Aminoglycoside	Gentamycin	28 (54.9 %)
	Tobramycin	12 (23.5 %)
	Netilmicin	8 (15.6 %)

Resistance profile (MDR) 38 (74.5 %).
($p < 0.0001$).

In the present study, 15.6 % of the isolates exhibited resistance to netilmicin. Notably, netilmicin retained effectiveness against nearly 75 % of *P. mirabilis* isolates, suggesting its potential as one of the most effective therapeutic agents against MDR-*P. mirabilis* and as a viable treatment option for carbapenem-resistant strains. However, these results contrast with findings from Iraq, where netilmicin displayed only modest activity (16.6 %) against *P. mirabilis* isolates, highlighting regional variations in susceptibility patterns. In addition, our analysis revealed a high resistance rate to imipenem, with 70.5 % (36/51) of isolates demonstrating resistance (Table 2). This outcome is particularly alarming given the clinical importance of carbapenems as last-resort antibiotics. Comparisons with previous research emphasize this concern: a study from Iraq reported that only 15 % of isolates were resistant to imipenem [72], while another study [2] found resistance in just four isolates using the disk diffusion method. Furthermore, another study [50] reported complete susceptibility of all *P. mirabilis* isolates to imipenem. The discrepancies across these studies may reflect differences in geographic distribution, antibiotic usage patterns, and methodological approaches. In contrast, cephalosporins such as ceftazidime, cefepime, and ceftriaxone showed moderate sensitivity (>50 %), consistent with previous results [51]. However, resistance to imipenem was alarmingly high at 70.5 % (Table 2), underscoring the rising prevalence of carbapenem resistance, which is a critical global public health threat [73]. Collectively, 74.5 % of isolates were resistant to at least three antimicrobial classes, confirming their MDR status, findings consistent with previous reports of high MDR prevalence in *P. mirabilis* [51].In recent years, the global prevalence of multidrug-resistant *P. mirabilis* isolates has shown a marked increase. Plasmids have been identified as playing a central role in mediating antimicrobial resistance in this species. Notably, many of these plasmids may possess a hybrid origin (cointegrate or mosaic structures), which significantly contributes to the dissemination of multiple antibiotic resistance genes across Enterobacterales populations [74]. This high prevalence of carbapenem resistance in the current study underscores a serious public health threat. Considering that carbapenems are often reserved for infections unresponsive to other antibiotic classes, the emergence of resistance in *P. mirabilis* significantly limits treatment options and calls for stricter antimicrobial stewardship, enhanced surveillance, and exploration of alternative therapeutic strategies [75].

3.4.2. Activity profiles of AuNPs against clinical pathogens

3.4.2.1. Determination of MIC and MBC of AuNPs against Gram-negative bacilli pathogens. The antibacterial potential of the biosynthesized AuNPs was assessed by determining their MIC and MBC against Gram-negative bacilli pathogens. The results of the MICs, MBCs, and MBC/MIC ratios are presented in Table 3. The MIC assays revealed that AuNPs exhibited the strongest antibacterial activity against *A. baumannii* and *P. mirabilis*, with MIC values of 156 μg/mL and 312 μg/mL, respectively. In contrast, *Klebsiella* sp. showed higher resistance, with a MIC of 1250 μg/mL. Both *E. coli* and *P. aeruginosa* displayed intermediate susceptibility, with MICs of 625 μg/mL. The corresponding MBCs for *E. coli*, *Klebsiella* sp., *P. aeruginosa*, *A. baumannii*, and *P. mirabilis* were 1250, 2500, 1250, 625, and 312 μg/mL, respectively. Importantly, the MBC/MIC ratio was consistently 2 for all tested isolates (Table 3).

Overall, these findings indicate that AuNPs synthesized from *P. mirabilis* possess strong antibacterial activity against Gram-negative pathogens, particularly *A. baumannii* and *P. mirabilis*. Their effectiveness can be attributed to their nanoscale size, which facilitates penetration and disruption of bacterial membranes [76]. In addition, the nanoparticles inhibited ATP production, with the highest suppression

Table 3
The MIC and MBC (μg/mL) as well as the tolerance ratio of strains of Gram-negative bacilli against AuNPs.

Nanoparticles	*E. coli*			*Klebsiella* sp.			*Pseudomonas aeruginosa*			*Acinetobacter baumannii*			*P. mirabilis*		
	MIC	MBC	Tolerance ratio	MIC	MBC	Tolerance ratio	MIC	MBC	Tolerance ratio	MIC	MBC	Tolerance ratio	MIC	MBC	Tolerance ratio
Au	625	1250	2	1250	2500	2	625	1250	2	312	625	2	156	312	2

observed in *P. mirabilis*, followed by *A. baumannii*, *E. coli*, and *P. aeruginosa*. When compared with a previous study [58], notable differences were observed, as that work reported much lower MIC (31.25 μg/mL) and MBC (500 μg/mL) values for *P. aeruginosa*.

3.4.2.2. Evaluation of the synergistic effect between antibiotics and biosynthesized AuNPs. The current study investigated the synergistic potential of biosynthesized AuNPs in combination with conventional antibiotics against Gram-negative bacilli pathogens. The antibacterial activities of ciprofloxacin (2 mg/mL), gentamicin (40 mg/mL), and ceftriaxone (100 mg/mL) were assessed individually and in combination with AuNPs using the microdilution broth method. The synergistic potential of biosynthesized AuNPs in combination with conventional antibiotics against Gram-negative bacilli pathogens demonstrated a reduction in optical density (OD 600 nm) compared with the control groups, confirming inhibitory effects on bacterial growth. Importantly, the antibiotics exhibited enhanced antibacterial activity when combined with AuNPs, resulting in a more pronounced suppression of Gram-negative bacilli growth (Fig. 3). The strongest inhibitory effect was recorded against *P. aeruginosa* isolates when ciprofloxacin, gentamicin, and ceftriaxone were used in conjunction with AuNPs. In contrast, the weakest inhibition under the same conditions was observed against *Klebsiella* sp. isolates. These findings align with previous work where bio-fabricated AuNPs conjugated with gentamycin, ciprofloxacin, rifampicin, and vancomycin showed enhanced efficacy against *Staphylococcus epidermidis* and *Staphylococcus haemolyticus* relative to antibiotics alone [77]. Collectively, these results reinforce the capacity of gold nanoparticles to potentiate the effects of β-lactams, cephalosporins, and aminoglycosides, validating earlier conclusions that AuNPs conjugated with small molecules such as drugs, vaccines, or antibodies are more effective than their unconjugated counterparts [78].

Moreover, the synergistic antibacterial effects observed are further supported by evidence from ceftriaxone-mediated AuNPs, which displayed potent activity against all tested bacterial pathogens in this study. Comparable findings were reported by an earlier study [79], who observed enhanced efficacy of ceftriaxone–AuNP conjugates against *A. baumannii* compared with either ceftriaxone or AuNPs alone. Similarly, another study [80] documented significant synergistic interactions ($P < 0.05$) between AuNPs and various antibiotics against *A. baumannii*, reporting excess inhibition zones of 24.79 %, 26.39 %, 22.99 %, 31.1 %, and 10.65 % for ceftazidime, ceftriaxone, ciprofloxacin, imipenem, and gentamicin, respectively.

The underlying mechanism of this enhanced antibacterial activity is thought to arise from microbe–metal interactions. The positive charge of nanoparticles promotes electrostatic attraction to the negatively charged bacterial cell surface, disrupting membrane permeability and facilitating nanoparticle entry. Once inside, nanoparticles may interfere with critical cellular processes including DNA, RNA, and protein synthesis [54]. Additionally, AuNPs may release ions that bind to thiol (-SH) groups of bacterial membrane transport proteins, thereby disrupting membrane function, respiration, and electron transport, ultimately leading to bacterial cell death [80]. Importantly, most studies indicate that functionalization of AuNPs with biomolecules such as antibiotics, peptides, or targeting ligands is critical for antibacterial efficacy. While bare AuNPs generally exhibit minimal effects on bacterial growth, conjugated forms significantly suppress bacterial proliferation and enhance drug performance [78]. This synergistic effect not only broadens the antimicrobial spectrum but also reduces antibiotic toxicity, restoring activity against resistant strains [81]. For instance, ampicillin-functionalized AgNPs and AuNPs demonstrated potent activity against MDR strains of *P. aeruginosa*, *Enterobacter aerogenes*, and MRSA, with ampicillin-capped AuNPs showing particularly strong bactericidal effects against resistant isolates (Brown et al., 2012).

Taken together, these findings highlight the promising potential of antibiotic-AuNP conjugates as novel therapeutics. By enhancing the effectiveness of conventional antibiotics and overcoming resistance mechanisms, AuNP-based nanocarrier systems may represent a crucial step forward in the development of alternative strategies to address the growing challenge of multidrug resistance.

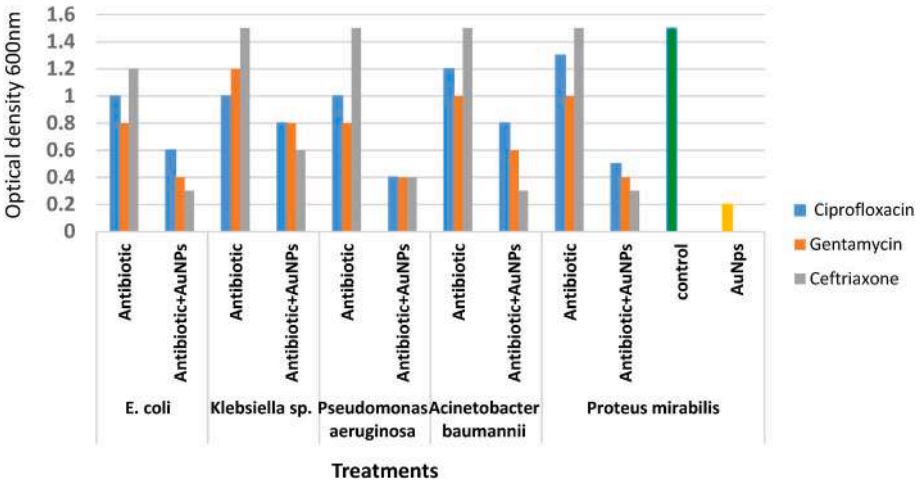

Fig. 3. Antibacterial activity of antibiotics alone and combined with gold nanoparticles against different bacterial strains. The optical density at 600 nm was measured for *E. coli*, *Klebsiella* sp., *Pseudomonas aeruginosa*, *Acinetobacter baumannii*, and *Proteus mirabilis* after treatment with ciprofloxacin, gentamycin, and ceftriaxone alone and in combination with AuNPs. Lower ODs in antibiotic + AuNP treatments reflect higher antibacterial potential as compared to the action of antibiotics alone. Control and AuNP alone have been included for comparison.

4. Conclusion and future direction

Accordingly, AuNPs synthesized by the bacterial isolate *P. mirabilis* hold tremendous potential as potent antibacterial agents against MDR Gram-negative pathogens. In the clinical analysis, the rate of bacterial isolation was highest in the sex distribution group (52.9 %) and lowest in the age group (9.8 %). Antimicrobial susceptibility testing indicated a high resistance rate to tigecycline at 88.2 % among the *P. mirabilis* isolates. The crystallite size of biosynthesized AuNPs as estimated for structural characterization was 12.5 nm, indicating diffraction planes for (111), (200), (220), and (311) as typical of a face-centered cubic lattice. Later, from the SEM study, an ellipsoidal morphology was evident, and FTIR spectroscopy confirmed the presence of amide and protein functional groups. The TEM analysis was performed and also showed the formation of nanoparticles with average sizes of ~6.21 nm. Functionally, *P. mirabilis*–derived AuNPs showed notable antibacterial activity against MDR Gram-negative strains, such as *P. aeruginosa*, *E. coli*, *A. baumannii*, and *P. mirabilis*. Synergistic studies also indicated increased inhibition of bacterial growth when AuNPs were used in combination with conventional antibiotics such as ceftriaxone, ciprofloxacin, and gentamicin, with the greatest synergy being observed against *P. aeruginosa*. In general, these findings establish that biosynthesized AuNPs are stable, biocompatible, and with the potential to enhance the efficacy of conventional antibiotics, hence acting as an adjuvant to antibiotics. Although the present study isolated 51 strains of *P. mirabilis* from various clinical specimens (blood, sputum, urine, etc.), therapeutic potential (wound healing, anaemia, antioxidant or oxidative-stress related disorders, and anti-cancer), optimization of dosage, safety, and pharmacokinetic profiles need further *in vivo* investigations and mechanistic studies. Therefore, the present study forms a foundational step toward the development of sustainable, green-synthesized nanomaterials in the fight against MDR bacterial infections and toward advanced antimicrobial therapies of the future.

4.1. Study limitations

Absence of *in vivo* toxicity data: The study did not assess *in vivo* biocompatibility, systemic toxicity, or pharmacokinetics of the biosynthesized AuNPs, which are critical for translational potential. This should be addressed in future studies.

CRediT authorship contribution statement

Kawther Hkeem Ibrahem: Writing – original draft, Methodology, Investigation, Formal analysis, Data curation, Conceptualization. **Sazan Moffaq Abdulaziz:** Writing – original draft, Methodology, Investigation, Formal analysis, Data curation, Conceptualization. **Sayran Hamad Haji:** Writing – original draft, Methodology, Investigation, Formal analysis, Data curation, Conceptualization. **Aryan R. Ganjo:** Writing – original draft, Supervision, Methodology, Formal analysis, Data curation, Conceptualization. **Nidhi Bhardwaj:** Writing – original draft, Methodology, Investigation, Formal analysis, Data curation, Conceptualization. **Indu Bhardwaj:** Writing – original draft, Methodology, Investigation, Formal analysis, Data curation, Conceptualization. **Soumya Ghosh:** Writing – review & editing, Writing – original draft, Visualization, Validation, Supervision.

Funding

This research did not receive any specific grant from funding agencies in the public, commercial, or not-for-profit sectors.

Declaration of competing interest

The authors declare that they have no known competing financial interests or personal relationships that could have appeared to influence the work reported in this paper.

Data availability

Data will be made available on request.

References

[1] M. ElTaweel, H.S. Said, R. Barwa, Emergence of extensive drug resistance and high prevalence of multidrug resistance among clinical Proteus mirabilis isolates in Egypt, Ann. Clin. Microbiol. Antimicrob. 23 (2024) 46.
[2] M.-F. Lin, M.-L. Liou, C.-H. Kuo, Y.-Y. Lin, J.-Y. Chen, H.-Y. Kuo, Antimicrobial susceptibility and molecular epidemiology of Proteus mirabilis isolates from three hospitals in Northern Taiwan, Microb. Drug Resist. 25 (2019) 1338–1346.
[3] E. Sharma, Y. Chen, C. Kelso, M. Sivakumar, G. Jiang, Carbapenems and colistin as last-resort antibiotics: a review of challenging environmental impacts and analytical methods, Soil Environ. Health (2024) 100058.
[4] A.R. Ganjo, F.A. Ali, S.T. Aka, B.M. Hussen, S.B. Smail, Diversity of biofilm-specific antimicrobial resistance genes in Pseudomonas aeruginosa recovered from various clinical isolates, Iran. J. Microbiol. 15 (2023) 742–749.
[5] C.S. Ho, C.T. Wong, T.T. Aung, R. Lakshminarayanan, J.S. Mehta, S. Rauz, et al., Antimicrobial resistance: a concise update, Lancet Microbe 6 (2025).
[6] V. Pareek, S. Devineau, S.K. Sivasankaran, A. Bhargava, J. Panwar, S. Srikumar, et al., Silver nanoparticles induce a triclosan-like antibacterial action mechanism in multi-drug resistant Klebsiella pneumoniae, Front. Microbiol. 12 (2021) 638640.
[7] N. Joudeh, D. Linke, Nanoparticle classification, physicochemical properties, characterization, and applications: a comprehensive review for biologists, J. Nanobiotechnol. 20 (2022) 262.
[8] M.K. Goshisht, Emerging nanomaterial strategies for antibacterial and antibiofilm applications: innovations in bacterial detection, mechanistic understanding, and therapeutic interventions to address antibiotic resistance, APMIS 133 (2025) e70050.
[9] X. Li, S.M. Robinson, A. Gupta, K. Saha, Z. Jiang, D.F. Moyano, et al., Functional gold nanoparticles as potent antimicrobial agents against multi-drug-resistant bacteria, ACS Nano 8 (2014) 10682–10686.
[10] A. Ahmeda, B. Mahdavi, F. Zaker, S. Kaviani, S. Hosseini, M.M. Zangeneh, et al., Chemical characterization and anti-hemolytic anemia potentials of tin nanoparticles synthesized by a green approach for bioremediation applications, Appl. Organomet. Chem. 34 (2020) e5433.
[11] A. Ahmeda, M.M. Zangeneh, A. Zangeneh, Green formulation and chemical characterization of lens culinaris seed aqueous extract conjugated gold nanoparticles for the treatment of acute myeloid leukemia in comparison to mitoxantrone in a leukemic mouse model, Appl. Organomet. Chem. 34 (2020) e5369.
[12] N. Abbasi, H. Ghaneialvar, R. Moradi, M.M. Zangeneh, A. Zangeneh, Formulation and characterization of a novel cutaneous wound healing ointment by silver nanoparticles containing citrus lemon leaf: a chemobiological study, Arab. J. Chem. 14 (2021) 103246.
[13] K. Ssekatawa, D.K. Byarugaba, C.D. Kato, F. Ejobi, R. Tweyongyere, M. Lubwama, et al., Nanotechnological solutions for controlling transmission and emergence of antimicrobial-resistant bacteria, future prospects, and challenges: a systematic review, J. Nanoparticle Res. 22 (2020) 117.
[14] B. Merchant, Gold, the noble metal and the paradoxes of its toxicology, Biologicals 26 (1998) 49–59.
[15] M. Borzenkov, P. Pallavicini, A. Taglietti, L. D'Alfonso, M. Collini, G. Chirico, Photothermally active nanoparticles as a promising tool for eliminating bacteria and biofilms, Beilstein J. Nanotechnol. 11 (2020) 1134–1146.
[16] M.A. Shaker, M.I. Shaaban, Formulation of carbapenems loaded gold nanoparticles to combat multi-antibiotic bacterial resistance: in vitro antibacterial study, Int. J. Pharm. 525 (2017) 71–84.
[17] L. Abdulazeem, Antibacterial, antibiofilm and antioxidant activity of gold nanoparticals biosynthesis of from local proteus mirabilis isolate, Elem. Educ. Online 20 (2021) 3336–3346.
[18] M. Abdoli, K. Sadrjavadi, E. Arkan, M.M. Zangeneh, S. Moradi, A. Zangeneh, et al., Polyvinyl alcohol/Gum tragacanth/graphene oxide composite nanofiber for antibiotic delivery, J. Drug Deliv. Sci. Technol. 60 (2020) 102044.
[19] A. Zangeneh, M.M. Zangeneh, R. Moradi, Ethnomedicinal plant-extract-assisted green synthesis of iron nanoparticles using Allium saralicum extract, and their antioxidant, cytotoxicity, antibacterial, antifungal and cutaneous wound-healing activities, Appl. Organomet. Chem. 34 (2020) e5247.
[20] Y. Li, N. Li, W. Jiang, G. Ma, M.M. Zangeneh, In situ decorated Au NPs on pectin-modified Fe3O4 NPs as a novel magnetic nanocomposite (Fe3O4/Pectin/Au) for catalytic reduction of nitroarenes and investigation of its anti-human lung cancer activities, Int. J. Biol. Macromol. 163 (2020) 2162–2171.
[21] L. Dou, X. Zhang, M.M. Zangeneh, Y. Zhang, Efficient biogenesis of Cu2O nanoparticles using extract of Camellia sinensis leaf: evaluation of catalytic, cytotoxicity, antioxidant, and anti-human ovarian cancer properties, Bioorg. Chem. 106 (2021) 104468.
[22] G. Mohammadi, M.M. Zangeneh, A. Zangeneh, Z.M.S. Haghighi, Chemical characterization and anti-breast cancer effects of silver nanoparticles using phoenix dactylifera seed ethanolic extract on 7, 12-Dimethylbenz [a] anthracene-induced mammary gland carcinogenesis in sprague dawley Male rats, Appl. Organomet. Chem. 34 (2020) e5136.

[23] W. Yan, Y. Liu, S. Mansooridara, A.S. Kalantari, N. Sadeghian, P. Taslimi, et al., Chemical characterization and neuroprotective properties of copper nanoparticles green-synthesized by nigella sativa L. seed aqueous extract against methadone-induced cell death in adrenal phaeochromocytoma (PC12) cell line, J. Exp. Nanosci. 15 (2020) 280–296.
[24] J. Liu, A. Zangeneh, M.M. Zangeneh, B. Guo, Antioxidant, cytotoxicity, anti-human esophageal squamous cell carcinoma, anti-human Caucasian esophageal carcinoma, anti-adenocarcinoma of the gastroesophageal junction, and anti-distal esophageal adenocarcinoma properties of gold nanoparticles green synthesized by Rhus coriaria L. fruit aqueous extract, J. Exp. Nanosci. 15 (2020) 202–216.
[25] Y. Han, Y. Gao, X. Cao, M.M. Zangeneh, S. Liu, J. Li, Ag NPs on chitosan-alginate coated magnetite for synthesis of indazolo [2, 1-b] phthalazines and human lung protective effects against α-Guttiferin, Int. J. Biol. Macromol. 164 (2020) 2974–2986.
[26] K. Ssekatawa, D.K. Byarugaba, C.D. Kato, F. Ejobi, R. Tweyongyere, M. Lubwama, et al., Nanotechnological solutions for controlling transmission and emergence of antimicrobial-resistant bacteria, future prospects, and challenges: a systematic review, J. Nanoparticle Res. 22 (2020) 1–30.
[27] H. Singh, J. Du, P. Singh, T.H. Yi, Extracellular synthesis of silver nanoparticles by Pseudomonas sp. THG-LS1. 4 and their antimicrobial application, J. Pharm. Anal. 8 (2018) 258–264.
[28] K.D. San Diego, J.I.A. Alindayu, R.Q. Baculi, Biosynthesis of gold nanoparticles by bacteria from hyperalkaline spring and evaluation of their inhibitory activity against pyocyanin production, J. Microbiol. Biotechnol. Food Sci. 2021 (2021) 781–787.
[29] Y. Cui, Y. Zhao, Y. Tian, W. Zhang, X. Lü, X. Jiang, The molecular mechanism of action of bactericidal gold nanoparticles on Escherichia coli, Biomaterials 33 (2012) 2327–2333.
[30] H. Kollenda, H. Frickmann, R.B. Helal, D.F. Wiemer, H. Naija, M.S. El Asli, et al., Screening for carbapenemases in ertapenem-resistant Enterobacteriaceae collected at a Tunisian hospital between 2014 and 2018, Eur. J. Microbiol. Immunol. 9 (2019) 9–13.
[31] A.A.G.A.M. Hezamb, M.M.A.I. Salih, Study the Effect of Different Temperatures on the Biofilm Production in Proteus mirabilis Isolated from Urinary Tract Infection Patients, 2020.
[32] T. Spilker, T. Coenye, P. Vandamme, J.J. LiPuma, PCR-based assay for differentiation of Pseudomonas aeruginosa from other Pseudomonas species recovered from cystic fibrosis patients, J. Clin. Microbiol. 42 (2004) 2074–2079.
[33] M.E. Altaai, I.H. Aziz, A.A. Marhoon, Identification Pseudomonas aeruginosa by 16s rRNA gene for differentiation from other Pseudomonas species that isolated from patients and environment, Baghdad Sci. J. 11 (2014) 1028–1034.
[34] S.F. Altschul, T.L. Madden, A.A. Schäffer, J. Zhang, Z. Zhang, W. Miller, et al., Gapped BLAST and PSI-BLAST: a new generation of protein database search programs, Nucleic Acids Res. 25 (1997) 3389–3402.
[35] K. Tamura, G. Stecher, S. Kumar, MEGA11: molecular evolutionary genetics analysis version 11, Mol. Biol. Evol. 38 (2021) 3022–3027.
[36] L. Abdulazeem, S.A. Jasim, S.A. Abdulrazzaq, Biosynthesis, characterization, anticancer activity and drug delivery of gold nanoparticles synthesised from local isolate of Proteus mirabilis, Res. J. Biotechnol. 17 (2022) 7.
[37] H. Barabadi, S. Honary, P. Ebrahimi, M.A. Mohammadi, A. Alizadeh, F. Naghibi, Microbial mediated preparation, characterization and optimization of gold nanoparticles, Braz. J. Microbiol. 45 (2014) 1493–1501.
[38] M. Khaleghi, S. Khorrami, H. Ravan, Identification of Bacillus thuringiensis bacterial strain isolated from the mine soil as a robust agent in the biosynthesis of silver nanoparticles with strong antibacterial and anti-biofilm activities, Biocatal. Agric. Biotechnol. 18 (2019) 101047.
[39] M. Peiris, S. Fernando, P. Jayaweera, N. Arachchi, T. Guansekara, Comparison of antimicrobial properties of silver nanoparticles synthesized from selected bacteria, Indian J. Microbiol. 58 (2018) 301–311.
[40] W. Hu, M. Li, W. Lu, S. Guo, J. Li, Evaluation of MASTDISCS combi carba plus for the identification of metallo-β-lactamases, KPC and OXA-48 carbapenemase genes in enterobacteriaceae clinical isolates, Lett. Appl. Microbiol. 70 (2020) 42–47.
[41] A.-P. Magiorakos, A. Srinivasan, R.B. Carey, Y. Carmeli, M. Falagas, C. Giske, et al., Multidrug-resistant, extensively drug-resistant and pandrug-resistant bacteria: an international expert proposal for interim standard definitions for acquired resistance, Clin. Microbiol. Infection 18 (2012) 268–281.
[42] M. Składanowski, M. Wypij, D. Laskowski, P. Golińska, H. Dahm, M. Rai, Silver and gold nanoparticles synthesized from streptomyces sp. isolated from acid forest soil with special reference to its antibacterial activity against pathogens, J. Cluster Sci. 28 (2017) 59–79.
[43] A.K. Mohammed, K.K. Salh, F.A. Ali, ZnO, TiO2 and Ag nanoparticles impact against some species of pathogenic bacteria and yeast, Cell. Mol. Biol. 67 (2021) 24–34.
[44] B. Das, S.K. Dash, D. Mandal, T. Ghosh, S. Chattopadhyay, S. Tripathy, et al., Green synthesized silver nanoparticles destroy multidrug resistant bacteria via reactive oxygen species mediated membrane damage, Arab. J. Chem. 10 (2017) 862–876.
[45] F. Abdel-Wahab, N. El Menofy, A. El-Batal, F. Mosallam, A. Abdulall, Enhanced antimicrobial activity of the combination of silver nanoparticles and different β Lactam antibiotics against methicillin resistant Staphylococcus aureus isolates, Azhar Int. J. Pharma. Med. Sci. 1 (2021) 22–31.
[46] L. Abdulazeem, B.H. Al-Amiedi, H.A. Alrubaei, Y.H. Al-Mawlah, Titanium dioxide nanoparticles as antibacterial agents against some pathogenic bacteria, Drug Invent. Today 12 (2019) 963–967.
[47] Y.P. Moreno Ruiz, L.A. de Almeida Campos, M.A. Alves Agreles, A. Galembeck, I. Macário Ferro Cavalcanti, Advanced hydrogels combined with silver and gold nanoparticles against antimicrobial resistance, Antibiotics 12 (2023) 104.
[48] J.N. Schaffer, M.M. Pearson, Proteus mirabilis and urinary tract infections, Microbiol. Spectr. 3 (2015).
[49] C.Y. Chen, Y.H. Chen, P.L. Lu, W.R. Lin, T.C. Chen, C.Y. Lin, Proteus mirabilis urinary tract infection and bacteremia: risk factors, clinical presentation, and outcomes, J. Microbiol. Immunol. Infect. 45 (2012) 228–236.
[50] D.A. Ahmed, Prevalence of Proteus spp. in some hospitals in Baghdad city, Iraqi J. Sci. (2015) 665–672.
[51] H. Owaied, S. Jabur, Antibiotic susceptibility of P. mirabilis isolated from clinical samples in Thi-Qar province, Univ.of Thi-Qar J. Sci. 9 (2022) 38–45.
[52] D.A. Ahmed, Prevalence of Proteus spp. in some hospitals in Baghdad city, Iraqi J. Sci. 56 (2023) 665–672.
[53] R. Mythili, T. Selvankumar, P. Srinivasan, A. Sengottaiyan, J. Sabastinraj, F. Ameen, et al., Biogenic synthesis, characterization and antibacterial activity of gold nanoparticles synthesised from vegetable waste, J. Mol. Liq. 262 (2018) 318–321.
[54] N. Rajput, A. Bankar, Bio-inspired gold nanoparticles synthesis and their anti-biofilm efficacy, J. Pharma. Investi. 47 (2017) 521–530.
[55] K. Chandran, S. Song, S.-I. Yun, Effect of size and shape controlled biogenic synthesis of gold nanoparticles and their mode of interactions against food borne bacterial pathogens, Arab. J. Chem. 12 (2019) 1994–2006.
[56] A. Chauhan, R. Verma, S. Kumari, A. Sharma, P. Shandilya, X. Li, et al., Photocatalytic dye degradation and antimicrobial activities of Pure and Ag-doped ZnO using Cannabis sativa leaf extract, Sci. Rep. 10 (2020) 7881.
[57] D. Sharma, A. Chauhan, R. Verma, P. Thakur, A.K. Mahajan, V. Kumar, et al., Structural, morphological, optical and biomedical applications of Berberis aristata mediated ZnO and Ag-ZnO nanoparticles, Nano Express 4 (2023) 045003.
[58] L. Abdulazeem, Biosynthesis of Gold Nanoparticals from Local Proteus mirabilis P242 Strain and Some Biological Application, 2020.
[59] T.L. Kalabegishvili, E.I. Kirkesali, A.N. Rcheulishvili, E.N. Ginturi, I.G. Murusidze, D.T. Pataraya, et al., Synthesis of gold nanoparticles by some strains of Arthrobacter genera, J. Mater. Sci. Eng.: Struct. Mater. Properties, Microstruct. Process. 2 (2012) 164–173.
[60] Y. Abdallah, M. Liu, S.O. Ogunyemi, T. Ahmed, H. Fouad, A. Abdelazez, et al., Bioinspired green synthesis of chitosan and zinc oxide nanoparticles with strong antibacterial activity against rice pathogen Xanthomonas oryzae pv. oryzae, Molecules 25 (2020) 4795.
[61] S. Pasieczna-Patkowska, M. Cichy, J. Flieger, Application of Fourier transform infrared (FTIR) spectroscopy in characterization of green synthesized nanoparticles, Molecules 30 (2025) 684.
[62] S.-H. Cha, Y. Park, J.W. Han, K. Kim, H.-S. Kim, H.-L. Jang, et al., Cold welding of gold nanoparticles on mica substrate: self-adjustment and enhanced diffusion, Sci. Rep. 6 (2016) 32951.
[63] M. Erasmus, O.A. Idris, A.I. Adetunji, E.D. Cason, Biogenic synthesis and characterization of gold nanoparticles using transformed mesophilic Escherichia coli BL21 and thermophilic Thermus thermophilus HB27, Biologia 79 (2024) 2605–2619.
[64] D.B. Manikandan, M. Arumugam, S. Veeran, A. Sridhar, R. Krishnasamy Sekar, B. Perumalsamy, et al., Biofabrication of ecofriendly copper oxide nanoparticles using Ocimum americanum aqueous leaf extract: analysis of in vitro antibacterial, anticancer, and photocatalytic activities, Environ. Sci. Pollut. Control Ser. 28 (2021) 33927–33941.
[65] I.M. Hasan, K.M. Abd-Elsabur, F.H. Assaf, M. Abd-Elsabour, Folic acid determination in food samples using green synthesized copper oxide nanoparticles and electro-poly (methyl orange) sensor, Electrocatalysis 13 (2022) 759–772.
[66] P.C. Mane, D.D. Kadam, A.N. Khadse, A.R. Chaudhari, S.P. Ughade, S.B. Agawane, et al., Green adeptness in synthesis of non-toxic copper and cobalt oxide nanocomposites with multifaceted bioactivities, Cancer Nanotechnol. 14 (2023) 79.
[67] A. Shelenkov, L. Petrova, V. Fomina, M. Zamyatin, Y. Mikhaylova, V. Akimkin, Multidrug-resistant Proteus mirabilis strain with cointegrate plasmid, Microorganisms 8 (2020).
[68] L. Lv, M. Wan, C. Wang, X. Gao, Q. Yang, S.R. Partridge, et al., Emergence of a plasmid-encoded resistance-nodulation-division efflux pump conferring resistance to multiple drugs, including tigecycline, in Klebsiella pneumoniae, mBio 11 (2020), https://doi.org/10.1128/mbio.02930-19.
[69] Z. Jiang, A New High-Throughput Assay for Quantification of Antibiotic Penetration in Gram-Negative Bacterial Cells, Syracuse University, 2020.
[70] R.G. Nelson, A. Rosowsky, Dicyclic and tricyclic diaminopyrimidine derivatives as potent inhibitors of cryptosporidium parvum dihydrofolate reductase: structure-activity and structure-selectivity correlations, Antimicrob. Agents Chemother. 46 (2002) 940.
[71] R. Zaman, S. Shamsuzzaman, In vitro and in vivo evaluation of antibiotic combinations against multidrug resistant Proteus mirabilis isolated from admitted patients of Dhaka Medical College Hospital, Dhaka, Arch. Microbiol. Immunol. 5 (2021).
[72] W.W. Al-Bassam, A.-K. Al-Kazaz, The isolation and characterization of Proteus mirabilis from different clinical samples, J. Biotechnol. Res. Center 7 (2013) 24–30.
[73] C. Jin, F. Zhou, Q. Cui, J. Qiang, C. An, Molecular characteristics of carbapenem-resistant Enterobacter cloacae in a tertiary hospital in China, Infect. Drug Resist. 13 (2020) 1575.
[74] A. Shelenkov, L. Petrova, V. Fomina, M. Zamyatin, Y. Mikhaylova, V. Akimkin, Multidrug-resistant Proteus mirabilis strain with cointegrate plasmid, Microorganisms 8 (2020) 1775.

[75] T. de Sousa, M. Hébraud, O. Alves, E. Costa, L. Maltez, J.E. Pereira, et al., Study of antimicrobial resistance, biofilm formation, and motility of Pseudomonas aeruginosa derived from urine samples, Microorganisms 11 (2023) 1345.
[76] Y. Rao, G.K. Inwati, M. Singh, Green synthesis of capped gold nanoparticles and their effect on Gram-positive and Gram-negative bacteria, Future Sci. OA 3 (2017) FSO239.
[77] S. Shaikh, N. Nazam, S.M.D. Rizvi, K. Ahmad, M.H. Baig, E.J. Lee, et al., Mechanistic insights into the antimicrobial actions of metallic nanoparticles and their implications for multidrug resistance, Int. J. Mol. Sci. 20 (2019).
[78] C. Tao, Antimicrobial activity and toxicity of gold nanoparticles: research progress, challenges and prospects, Lett. Appl. Microbiol. 67 (2018) 537–543.
[79] S.M.F. Gad El-Rab, E.M. Halawani, A. Hassan, Formulation of ceftriaxone conjugated gold nanoparticles and their medical applications against extended-spectrum β-Lactamase producing bacteria and breast cancer, J. Microbiol. Biotechnol. 28 (2018) 1563–1572.
[80] Al-Shaabani, et al., ECO-FRIENLY synthesis of gold nanoparticles and study their effect with antibiotics against acinetobacter baumannii, Iraqi J. Agric. Sci. 51 (2020) 1204–1211.
[81] M. Rai, A.P. Ingle, R. Pandit, P. Paralikar, I. Gupta, M.V. Chaud, et al., Broadening the spectrum of small-molecule antibacterials by metallic nanoparticles to overcome microbial resistance, Int. J. Pharm. 532 (2017) 139–148.